

Rethinking deinterlacing for early interlaced videos

Yang Zhao, Wei Jia, Ronggang Wang

Abstract—In recent years, high-definition restoration of early videos have received much attention. Real-world interlaced videos usually contain various degradations mixed with interlacing artifacts, such as noises and compression artifacts. Unfortunately, traditional deinterlacing methods only focus on the inverse process of interlacing scanning, and cannot remove these complex and complicated artifacts. Hence, this paper proposes an image deinterlacing network (DIN), which is specifically designed for joint removal of interlacing mixed with other artifacts. The DIN is composed of two stages, *i.e.*, a cooperative vertical interpolation stage for splitting and fully using the information of adjacent fields, and a field-merging stage to perceive movements and suppress ghost artifacts. Experimental results demonstrate the effectiveness of the proposed DIN on both synthetic and real-world test sets.

Index Terms—deinterlacing, early videos, interlacing artifacts

I. INTRODUCTION

Interlacing artifacts are commonly observed in many early videos, which are caused by interlacing scanning in early television systems, *e.g.*, NTSC, PAL, and SECAM. As shown in Fig. 1, the odd lines and even lines of an interlaced frame are scanned from two different half-frames, *i.e.*, the odd/top/first field and the even/bottom/second field. The two fields cannot be exactly aligned; hence, comb teeth aliasing appears in these different areas, especially when there are large movements between the two fields. With the rapid development of image restoration techniques, high-definition reconstruction of early videos has achieved impressive results. However, there are few studies about the interlacing artifacts removal that often appear in early videos.

Traditional deinterlacing methods [1], [2] are mainly designed for simple interlacing scanning process. Unfortunately, interlaced effects are often mixed with many other unnatural artifacts in real-world early videos, such as blocking and noise during compression, transfer, and storage. The performances of traditional deinterlacing methods thus often significantly decrease. Additionally, recent state-of-the-art (SOTA) image restoration models are not specifically designed for this artificial interlaced mechanism. As a result, the motivation of

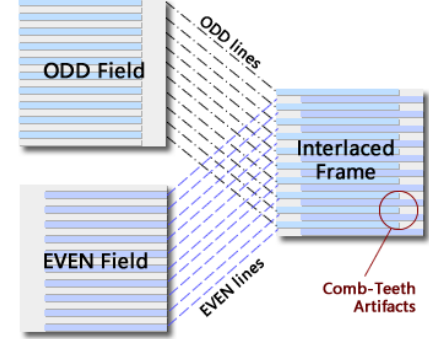


Fig. 1. Illustration of the interlaced scanning mechanism.

this paper is to specifically design an effective deinterlacing network for the joint restoration tasks of interlaced frames.

The traditional interlaced scanning mechanism can be defined as $\mathbf{Y} = S(\mathbf{X}_1, \mathbf{X}_2)$, where \mathbf{Y} denotes the interlaced frame, $S(\cdot)$ is the interlaced scanning function, and $\mathbf{X}_1, \mathbf{X}_2$ denote the odd and even fields. Traditional deinterlacing methods focus on the reversed process of $S(\cdot)$, which can be roughly divided into four categories, *i.e.*, temporal interpolation, spatial interpolation, motion-based approaches, and learning-based methods. Temporal interpolation-based deinterlacing utilizes adjacent frames to interpolate the missing lines. However, the differences between two frames lead to visible artifacts when there are large movements in adjacent frames. Spatial interpolation is another kind of basic deinterlacing technique that adopts only one field to estimate the whole frame. The simplest spatial interpolation is the line average and edge line average. Various single field interpolation methods have been proposed in the past decades, for instance, edge detection with fuzzy logic [3], block-wise autoregression [4], bilateral filtering model [5], locality and similarity adaption [6], the maximum a posteriori model [7] and least square methods [8]. To further refine the visual quality, visual saliency is also introduced to improve deinterlacing, for example, spectral residual visual saliency-based deinterlacing [9], [10]. There are also some single field interpolation methods for special applications, such as GPU-parallel implementation of edge-directed interpolation [11] and deinterlacing for 1080p-to-8KUHD [12]. To improve deinterlacing methods for large movements, motion-based methods have been proposed to make use of two fields [13]–[15] or adaptively improve single field methods [16], [17]. Many motion-compensation-based methods have also been introduced to calculate motion vectors between two frames to estimate the movements. Proper temporal or spatial interpolations are then applied according to the estimated movements [18]–[20], [37], [38]. Recent dictionary learning-based models have also been applied for

This work is supported by the National Natural Science Foundation of China (Nos.61972129, 62072013, 62076086), and Shenzhen Research Projects of JCYJ20180503182128089, 201806080921419290, RC JC20200714114435057, GXWD20201231165807007-20200806163656003. R. Wang is the corresponding author.

Y. Zhao and W. Jia are with School of Computer and Information, Hefei University of Technology, Hefei 230009, China (e-mail: yzhao@hfut.edu.cn; jiawei@hfut.edu.cn).

R. Wang is with the School of Electronic and Computer Engineering, Peking University Shenzhen Graduate School, 2199 Lishui Road, Shenzhen 518055, China (e-mail: rgwang@pksuz.edu.cn).

Y. Zhao and R. Wang are also with Peng Cheng National Laboratory, Shenzhen 518000, China.

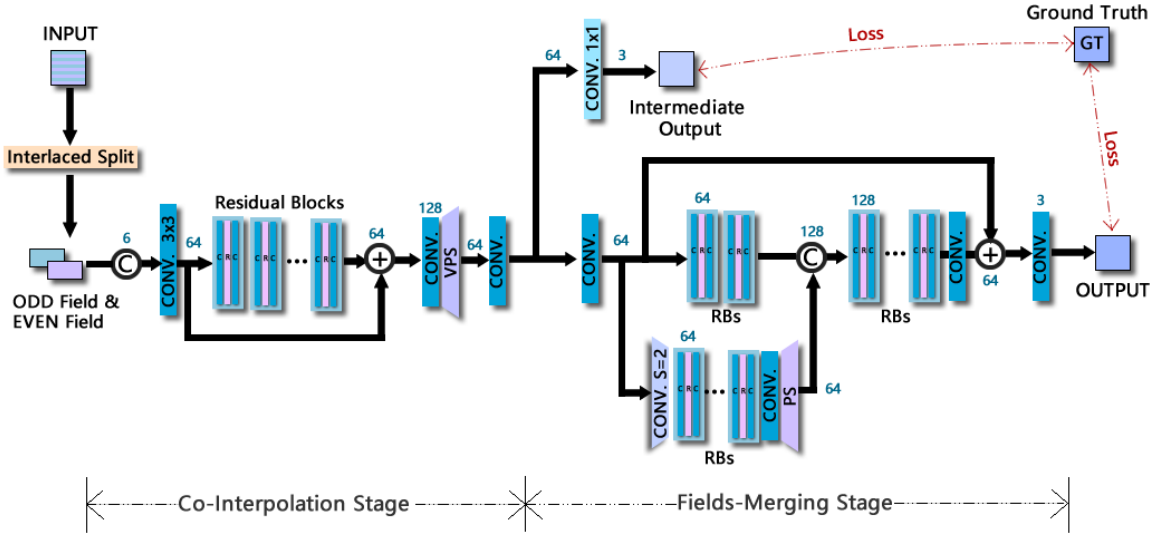


Fig. 2. Architecture of the proposed deinterlacing network.

deinterlacing, *e.g.*, Choi et al. [21] used a joint dictionary learning method to reconstruct interlaced high dynamic range video. With the explosion of deep neural network (DNN)-based methods in many low-level vision tasks [22], [23], [27]–[29], Zhu et al. [30] first introduced a lightweight deinterlacing convolutional neural network (DICNN) to deinterlacing task based on a shallow super-resolution CNN (SRCNN) architecture [23]. Liu et al. [35] further improved DICNN by using a deformable convolution and attention-residual-blocks. Bernasconi et al. [36] presented an effective multi-field deinterlacing method based on residual dense network. In [34], Akyüz proposed a residual network with dilated convolutions for joint deinterlacing and denoising of dual-ISO HDR images. However, these approaches are mainly focused on reverse of interlacing scanning and still cannot handle the complex and complicated artifacts in real-world early videos. In this paper, the degradation process of interlaced early video is computed as $Y = C(S(X_1, X_2)) + n$, where $C(\cdot)$ denotes the video compression and n represents multiple noise. Hence, the proposed image deinterlacing method should jointly consider the complex interlacing artifacts mixed with other compression artifacts and noise.

To address this problem, a deinterlacing network (DIN) is specifically designed based on the analysis of the traditional interlacing scanning mechanism. The proposed DIN consists of two stages: the co-interpolation stage and the field-merging stage. In the co-interpolation stage, the input frame is first divided into odd field and even field, and then the two fields are simultaneously inputted into a ResNet to implement vertical interpolation. Hence, the network can clearly know that these two fields are from two different frames and can still make use of the mutual latent features since these two frames have many similar contents. Additionally, the vertical pixel-shuffling module is adopted to simulate the interlaced scanning process. In the field-merging stage, the interpolated field features are fused to the final output. The ResNet structure is selected to avoid the loss of high-frequency details. Note that larger receptive

fields are needed in this stage for perceiving the movements and removing the ghost artifacts of the merged frame. Another downscale and reconstruction branch is thus added to achieve a larger receptive field. Note that it is difficult to obtain ground truth for early videos, and we train the proposed DIN on a synthetic datasets and test it on both the synthetic datasets and real-world early video frames.

II. THE PROPOSED METHOD

A. Architecture of the Deinterlacing Network

Different from many image restoration tasks that have blind degradation models, interlaced scanning is a fixed artificial mechanism. Hence, the network is specially designed according to the characteristics of interlaced scanning. The architecture of the proposed DIN is illustrated in Fig. 2, which consists of two stages, *i.e.*, the co-interpolation stage (CIS) and the fields-merging stage (FMS). In the following, each stage is introduced and analysed in detail.

B. Co-Interpolation Stage

The main purpose of CIS is to compute the vertical interpolation of two fields, and its structure is illustrated in detail in Fig. 2. An effective enhanced super-resolution network (EDSR) [27], [28] is adopted as the backbone of CIS, which utilizes a typical ResNet structure [31] and carefully optimizes the residual blocks for image restoration tasks. Note that we do not use ResNet as a blackbox to entirely reconstruct interlaced frame, and do not first recover the interlaced fields and then apply interlacing scanning as in DICNN [30] either. In the proposed DIN, the input frame is first split into even field and odd field according to the interlacing mechanism, which contain even lines and odd lines, respectively. There are mainly two benefits of this split and co-interpolation subnetwork. First, instead of the whole frame that contains serious comb teeth artifacts, the odd and even fields are used as input. Hence, the disruption of interlacing artifacts is minimized during the

training of the DIN. Second, the two adjacent fields have considerable similar spatial information. As a result, the two fields are inputted simultaneously into the network, which is helpful to recover the high-frequency pixel-level details.

Additionally, the split fields have half the size of the original frame. Motivated by the efficient pixel-shuffling (PS) module [26], which is widely adopted in current SOTA super-resolution methods [24], [27], [28] to reduce the computational cost, the CIS also reconstructs the fields in low-resolution space and then utilizes a vertical pixel shuffling (VPS) at the end of the network to magnify the reconstructed features. Similar to the traditional interlacing scanning mechanism in Fig. 1, the VPS module interlacedly combine odd lines and even lines into an entire frame, which can be regarded as a special case of a normal PS module.

In our experiment, the CIS contains 6 residual blocks (RB). Each RB consists of a 3×3 convolutional layer (conv.), a rectified linear unit (ReLU) activation, another conv. 3×3 , and a local residual connection, as in [27]. The common global skip is used to improve the convergence of deep ResNet.

C. Fields-Merging Stage

The most significant artifact in the deinterlacing process is caused by the large movement between two fields. Hence, the subnetwork of the FMS tends to have a large receptive field to perceive movement information. Note that some commonly used architectures with large receptive fields, *e.g.*, UNet and autoencoder, often lead to the loss of pixelwise spatial details. Hence, the proposed FMS applies multiscale ResNet, which utilizes a base ResNet to maintain pixel-level information and then adds a downscale branch to perceive larger-scale movements. The final feature of the downscale branch is magnified via a PS module and then concatenated to the middle of the base ResNet.

By means of the two-scale structure, the proposed FMS can effectively preserve high-frequency details and extract differences at a larger scale simultaneously. As shown in Fig. 2, in our experiment, 3 RBs are used in the downscale branch; conv. 3×3 with stride 2 is utilized as the downsampling module, and the 2×2 PS module is adopted for upsampling after RBs. The base branch contains 5 RBs, which have 2 RBs before the concatenation of the downscale branch, and 3 RBs after the concatenation. The global skip connection is also used. In general, adding more scales can extract higher-level semantic information and perceive larger movement. However, the parameters and computational cost also increase accordingly. In our experiment, we have observed that two-scale FMS can already handle the deinterlacing task well. Hence, for keeping simplicity, only two scales are used in the proposed DIN.

D. Loss Function of the DIN

Similar to many image restoration models, the proposed DIN is end-to-end trained via a L_1 -distance-based loss function. As shown in Fig. 2, the two stages of the DIN are both supervised by the ground truth data. To constrain the interpolated field features by means of single ground truth,

a temporary conv. 1×1 is used to linearly combine the interpolated field features (64 channels) to the intermediate output. This supervision of intermediate output is added to directly optimize the CIS module and better train the co-interpolation stage. The entire network is then optimized by means of the following loss function:

$$L = \frac{1}{N_T} \sum_{n=1}^{N_T} [\lambda \|C_1(F_{CIS}(\mathbf{X}_1^n, \mathbf{X}_2^n)) - \mathbf{Y}^n\|_1 + (1 - \lambda) \|F_{FMS}(F_{CIS}(\mathbf{X}_1^n, \mathbf{X}_2^n)) - \mathbf{Y}^n\|_1], \quad (1)$$

where N_T denotes the total number of training samples, $\mathbf{X}_1^n, \mathbf{X}_2^n$ are the odd and even fields, \mathbf{Y}^n represents the ground truth frame, C_1 is the conv. 1×1 operation, F_{CIS} and F_{FMS} denote subnetworks of CIS and FMS, respectively, and λ is an artificial weight of the intermediate supervision. This weight λ is initially set as 0.5, so the CIS module can be constrained to recover better vertical interpolation results. Then, the λ is gradually reduced to 0.1 in the last half of the training phase.

E. Implementational Details

In our experiment, a total of 100,000 training patch pairs with a size of 256×256 are selected from the training set, and then these patches are augmented via horizontal and vertical flipping. It should be noted that rotation cannot be used for data augmentation in deinterlacing because the interlaced artifacts are along the horizontal direction. In this paper, each conv. layer in RBs outputs 64 feature maps except for the last 3 RBs in FMS, which have 128 channels after the concat operation. The weights are initialized via Xavier, and the network is optimized via Adam. The initial learning rate is 10^{-4} and then decreases by a factor of 10 after every 20 epochs. This network was trained 100 epochs with a GTX1080Ti GPU by means of the MXNET platform.

III. EXPERIMENTS

A. Training and Testing Datasets

For training, a total of 400 video sequences are collected from the YOUKU-2K video dataset [32]. Each video sequence consists of 100 frames with 2K resolution. Then, the interlaced frame is produced according to the traditional interlaced scanning system, *i.e.*, the odd and even lines are scanned from two adjacent frames. The real first frame is utilized as ground truth data. Furthermore, the interlaced video is then compressed via the H.264 codec with a random “-crf” parameter from 30 to 38 by means of FFmpeg tool. This compression process is adopted to roughly simulate the mixed compression artifacts in early videos.

For testing, we used three synthetic test sets and a real-world early video dataset. In the synthetic test sets, 40 frames from YOUKU-2K dataset, 75 frames from REDS validation set [40] and 225 frames from VIMEO90K dataset [39] are randomly selected for testing. All the testing frames are generated in the same way as in the training stage. In the real-world dataset, 38 interlaced frames are randomly selected from several real-world early videos to verify the generalization of the DIN.

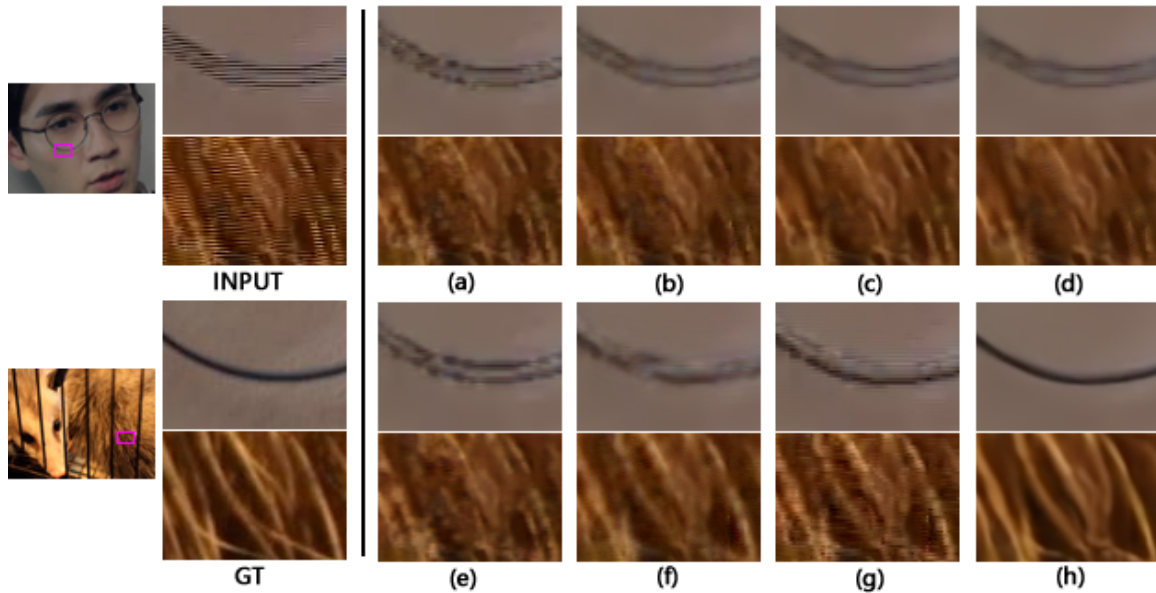


Fig. 3. Deinterlacing results on synthetic YOUKU-2K dataset, (a) retrained SRCNN [23] (b) retrained EDSR [27], (c) retrained RCAN [24], (d) retrained RDN [25], (e) DICNN [30], (f) retrained DJDD [34], (g) retrained STCLN [35], (h) the proposed DIN.

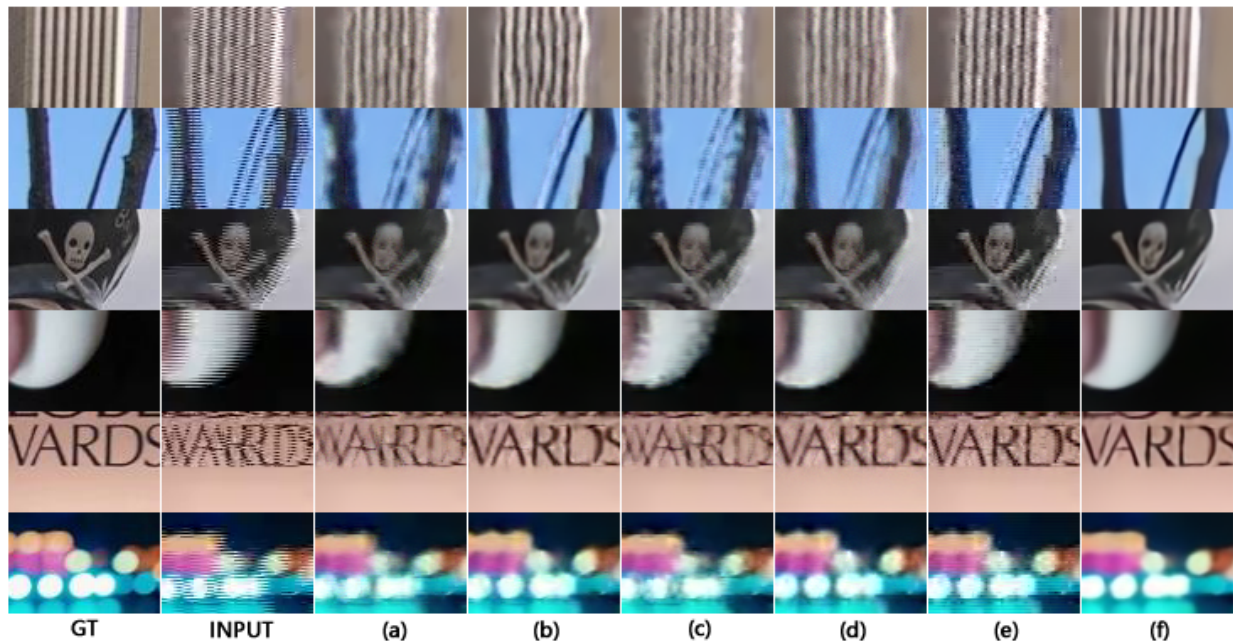


Fig. 4. Deinterlacing results on synthetic REDS and VIMEO90K datasets, (a) retrained EDSR [27], (b) retrained RDN [25], (c) DICNN [30], (d) retrained DJDD [34], (e) retrained STCLN [35], (f) the proposed DIN.

B. Experimental Results on the Synthetic Testing Sets

In our experiment, the proposed DIN is compared with deep deinterlacing models of DICNN [30], DJDD (deep joint deinterlacing and denoising network) [34], STCLN (spatial-temporal correlation learning network) [35], and several image restoration networks, e.g., super-resolution models SRCNN [23], EDSR [27], RCAN [24], and denoise model RDN [25]. For a fair comparison, these networks are all retrained with the same training set. Note that the PS upsampling module in EDSR and RCAN is not used because the resolution is

not magnified. In addition, single field interpolation is also compared by using EDSR [27] as upsampling method.

Fig. 3 illustrates the results of several interlaced and compressed frames in YOUKU-2K set. First, retrained SOTA models of EDSR, RCAN, RDN and DJDD can reduce interlacing and compression noise, but they still cause blur or ghost artifacts. Second, lightweight DICNN and STCLN, which are designed for deinterlacing without noise, directly combine reconstructed fields with original noisy fields. Therefore, they cannot remove these mixed artifacts. Last, the DIN can remove interlacing and compression artifacts simultaneously.

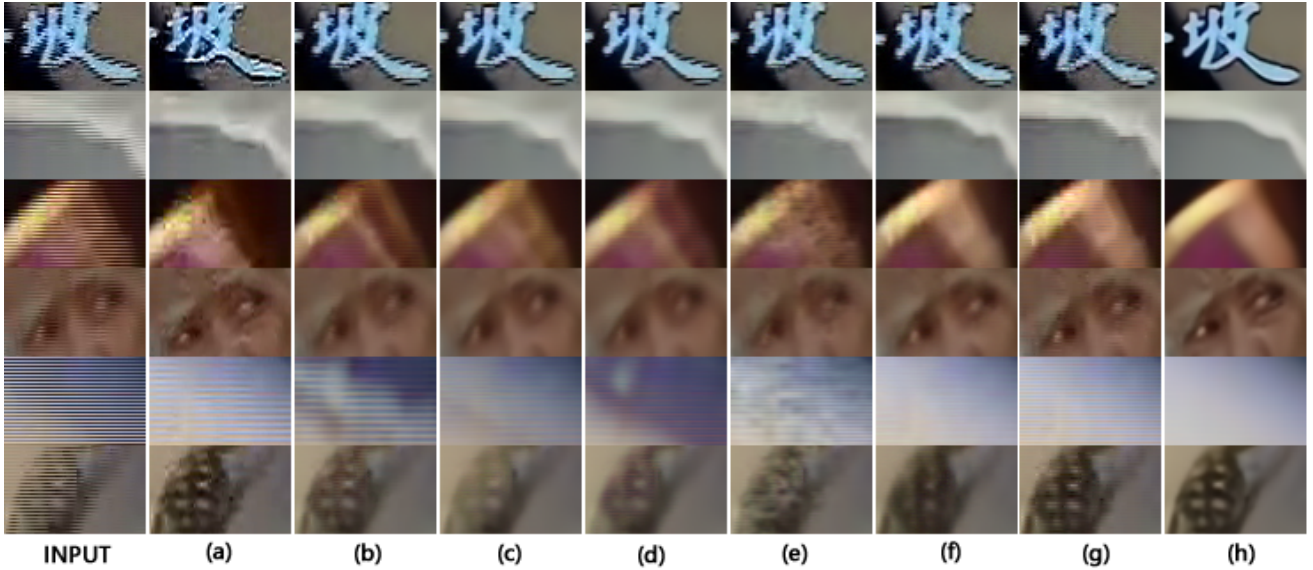


Fig. 5. Reconstruction results of real-world early video frames with different methods, (a) single field EDSR [27], (b) retrained EDSR [27], (c) retrained RCAN [24], (d) retrained RDN [25], (e) DICNN [30], (f) retrained DJDD [34], (g) retrained STCLN [35], (h) the proposed DIN.

TABLE I
PSNR AND SSIM RESULTS ON THE SYNTHETIC YOUKU-2K DATASET

	PSNR	SSIM	Number of Param.
Input	30.33	0.8777	-
Single Field EDSR	32.04	0.9088	5.905M
SRCNN (retrain) [23]	32.43	0.9111	0.036M
EDSR (retrain) [27]	32.65	0.9130	5.905M
RCAN (retrain) [24]	32.45	0.9168	5.066M
RDN (retrain) [25]	32.60	0.9178	2.375M
DICNN [30]	32.53	0.9125	0.118M
DJDD [34]	33.23	0.9211	0.925M
STCLN [35]	32.84	0.9124	0.351M
DIN	35.17	0.9348	1.816M

TABLE II
PSNR AND SSIM RESULTS ON THE SYNTHETIC REDS AND VIMEO90K DATASETS

	REDS		VIMEO90K	
	PSNR	SSIM	PSNR	SSIM
Input	24.79	0.7059	25.05	0.7697
EDSR(retrain) [27]	26.14	0.7437	26.94	0.8291
RCAN(retrain) [24]	27.49	0.7797	29.66	0.8690
RDN(retrain) [25]	27.81	0.7828	29.87	0.8714
DICNN [30]	26.06	0.7397	26.64	0.8208
DJDD [34]	26.56	0.7549	28.91	0.8548
STCLN [35]	27.27	0.7573	29.25	0.8390
DIN	28.17	0.8007	30.34	0.8827

Fig. 4 shows results on REDS and VEMIO90K test sets. The RDN and DJDD can reproduce better results for large motion than EDSR and shallow DICNN. However, they still cannot suppress complex artifacts mixed with interlacing. The STCLN can reduce ghost artifact by means of deformable convolution, but it still reproduces severe noises. By comparing the visual quality, the proposed DIN obtains cleaner and more natural results than these SOTA models.

Related objective assessments are listed in Table I and Table II. The DIN outperforms other DNN-based methods on these synthetic test sets. Note that the DICNN and STCLN

are designed for real-time deinterlacing task, which are very lightweight base on shallow backbones. By comparing with directly applying deeper model of EDSR, RCAN and RDN, which are not specifically designed for joint deinterlacing task, the DIN performs more effective with fields split, co-interpolation and fields merging mechanism.

C. Experimental Results on Real-World Early Videos

Fig. 5 shows the reconstructed results of real-world early video frames. There is considerable aliasing and compression noise in these frames. First, the single field EDSR avoids comb teeth but also magnifies aliasing during vertical interpolation. Second, the lightweight DICNN and STCLN cannot totally remove mixed noise and aliasing. Third, the SOTA models of EDSR, RCAN and RDN can reduce interlacing and compression artifacts, however, they still lead to ghost shadows and blurry results. Fourth, the DJDD can suppress ghost artifacts, but the results of DJDD also contain blur or noise. Finally, although these models are trained on the same dataset, the DIN can significantly remove interlacing mixed with noises, which demonstrates that the proposed method is effective for these real-world early videos.

Single stimulus subjective testing has been applied to compare the visual quality of reconstructed early videos. The details of the viewing conditions and test session are set according to Rec. ITU-R BT.500 [33]. A total of 15 observers are invited to score the impairment scales of six sets of frames to 5 levels, where the impairment levels 5, 4, 3, 2, and 1 denote “imperceptible impairment”, “perceptible impairment”, “slightly annoying impairment”, “annoying impairment”, and “very annoying impairment”, respectively. The average impairment scale scores (ISS) are listed in Table III. It can be easily found that the proposed method achieves much higher subjective scores than other methods. Scores of two DNN-based blind image quality assessment (BIQA) methods, *i.e.*,

TABLE III

BIQA AND IMPAIRMENT SCALE SCORES ON REAL-WORLD EARLY VIDEOS

	HyperIQA	KonIQ	ISS	Time (s)
Input	28.47	41.68	2.14	-
EDSR (retrain) [27]	29.08	41.34	2.85	0.77
RCAN (retrain) [24]	28.91	41.67	3.12	1.34
RDN (retrain) [25]	28.81	41.63	2.82	1.44
DICNN [30]	29.09	41.69	2.54	0.08
DJDD [34]	28.95	41.67	3.65	1.16
STCLN [35]	29.04	41.82	2.70	0.12
DIN	29.32	42.91	4.33	0.73

HyperIQA [41] and KonIQ [42], are also listed in Table III. Compared with other SOTA models, DIN can achieve higher results. Note that these BIQA methods are not trained with interlaced degradations. Therefore, these BIQA scores are only used for rough comparisons, and are not completely consistent with visual quality. In addition, average running time of different methods is also listed in Table III. Lightweight DICNN and STCLN run much faster than other deep models. By comparing with other deeper models, the DIN can achieve better results with less time cost. (More results can be found in supplementary materials: <https://gitee.com/gityzhao/din/>)

IV. CONCLUSION

This paper proposes a deinterlacing network (DIN) for early videos that contains interlacing and mixed compression artifacts. The two-stage architecture of the proposed DIN is motivated by the interlacing scanning mechanism and traditional deinterlacing strategies. The co-interpolation stage splits the interlaced frame into odd and even fields and then estimates the vertical interpolation of two fields. Another field-merging stage is then applied to further remove ghost shadows and other unnatural artifacts. Experimental results demonstrate that the DIN can effectively recover high-quality results from interlaced and compressed frames.

REFERENCES

- [1] D. Gerard, and E. Bellers. "Deinterlacing-an overview," *Proc. IEEE*, vol. 86, no.9, pp.1839-1857, 1998.
- [2] T. Doyle, "Interlaced to sequential conversion for EDTV applications," in *Proc. International Workshop on Signal Processing of HDTV*, 1990, pp. 412-430.
- [3] P. Brox, I. Baturone, S. Solano, and J. Rios, "Edge-adaptive spatial video deinterlacing algorithms based on fuzzy logic," *IEEE Trans. Consumer Electronics*, vol. 60, no. 3, pp.375-383, 2014.
- [4] J. Wang, G. Jeon, J. Jeong, "A block-wise autoregression-based deinterlacing algorithm," *Journal of Display Technology*, vol.10, no.5, pp.414-419, 2013.
- [5] V. Jakhetiya, O. C. Au, S. Jaiswal, L. Jia, H. Zhang, "Fast and efficient intra-frame deinterlacing using observation model based bilateral filter," *Int. Conf. Acoustics, Speech and Signal Process.*, 2014, pp.5819-5823.
- [6] J. Wang, J. Gwanggil, and J. Jechang, "Efficient adaptive deinterlacing algorithm with awareness of closeness and similarity," *Optical Engineering*, vol.51, no.1, 017003-1, 2012.
- [7] J. Wang, J. Gwanggil, and J. Jechang, "De-Interlacing algorithm using weighted least squares," *IEEE Trans. Circuits and Syst. Video Technol.*, vol.24, no.1, pp.39-48, 2014.
- [8] J. Wang, J. Gwanggil, and J. Jechang, "Moving least-squares method for interlaced to progressive scanning format conversion," *IEEE Trans. Circuits and Syst. Video Technol.*, vol.23, no.11, pp.1865-1872, 2013.
- [9] U. Aggarwal, M. Trocan, F. Coudoux, "Spectral saliency-based video deinterlacing," *International Conference on Computational Collective Intelligence*, 2016, pp. 590-598.
- [10] U. Aggarwal, M. Trocan, F. Coudoux, "An HVS-inspired video deinterlacer based on visual saliency," *Vietnam Journal of Computer Science*, vol. 4, pp.61-69, 2017.
- [11] J. Wu, Z. Song, G. Jeon, "GPU-parallel implementation of the edge-directed adaptive intra-field deinterlacing method," *Journal of Display Technology*, vol.10, no.9, pp.746-753, 2014.
- [12] Y. Chang and C. Fan, "Spatial-domain edge-directed interpolation based deinterlacing to up-scaling technology for 1080i full HD to progressive 8K ultra HD," *Int. Conf. Consumer Electronics*, 2017, pp. 275-276.
- [13] D. Wang, A. Vincent, and P. Blanchfield, "Hybrid de-interlacing algorithm based on motion vector," *IEEE Trans. Circuits Syst. Video Technol.*, vol. 15, no. 8, pp. 1019-1025, Aug. 2005
- [14] D. Hargreaves and J. Vaisey, "Bayesian motion estimation and interpolation in the interlaced video sequences," *IEEE Trans. Image Process.*, vol. 6, no. 5, pp. 764-769, May 1997.
- [15] P. Brox, I. Baturone, and S. Sanchez-Solano, "Fuzzy motion-adaptive interpolation with picture repetition detection for deinterlacing," *IEEE Trans. Instrum. Meas.*, vol. 58, no. 9, pp. 2952-2958, Sep. 2009.
- [16] K. Lee and C. Lee, "High quality spatially registered vertical temporal filtering for deinterlacing," *IEEE Trans. Consumer Electronics*, vol.59, no.1, pp.182-190, 2013.
- [17] X. Zhang and D. Wang, D, "An efficient motion adaptive deinterlacing algorithm using improved edge-based line average interpolation," *IEEE Int. Conf. Signal Process.*, 2016, pp. 659-662.
- [18] H. M. Mohammadi, Y. Savaria, and J. M. P. Langlois, "Enhanced motion compensated deinterlacing algorithm," *IET Image Process.*, vol. 6, no. 8, pp. 1041-1048, Nov. 2012.
- [19] G. Jeon, J. You, and J. Jeong, "Weighted fuzzy reasoning scheme for interlaced to progressive conversion," *IEEE Trans. Circuits and Syst. Video Technol.*, vol.19, no.6, pp.842-855, 2009.
- [20] X. Zhu, Q. Huang, F. Ye, F. Liu, S. Xu, Y. Wang, Y, "Motion-compensated deinterlacing based on scene change detection," *Pacific Rim Conference on Multimedia*, Cham, 2017, pp. 397-406.
- [21] I. Choi, S. Baek, M. Kim, "Reconstructing interlaced high-dynamic-range video using joint learning," *IEEE Trans. Image Process.*, vol.26, no.11, pp.5353-5366, 2017.
- [22] K. Zhang, W. Zuo, Y. Chen, D. Meng and L. Zhang, "Beyond a gaussian denoiser: Residual learning of deep cnn for image denoising," *IEEE Trans. Image Process.*, vol.26, no.7, pp.3142-3155, 2017.
- [23] C. Dong, C. Loy, K. He and X. Tang, "Image super-resolution using deep convolutional networks," *IEEE Trans. Pattern Anal. Mach. Intell.*, vol. 38, no. 2, pp. 295-307, Jul. 2016.
- [24] Y. Zhang, K. Li, K. Li, L. Wang, B. Zhong and Y. Fu, "Image super-resolution using very deep residual channel attention networks," in *Proc. Euro. Conf. Comput. Vis.*, Sept. 2018.
- [25] Y. Zhang, Y. Tian, Y. Kong, B. Zhong and Y. Fu, "Residual Dense Network for Image Restoration," *IEEE Trans. Pattern Anal. Mach. Intell.*, vol. 43, no. 7, pp. 2480-2495, 2021.
- [26] W. Shi, J. Caballer, et al., "Real-Time single image and video super-resolution using an efficient sub-pixel convolutional neural network," *IEEE Conf. Comput. Vis. Pattern Recognit.*, 2016, pp. 1874-1883.
- [27] B. Lim, S. Son, H. Kim, S. Nah and K. M. Lee, "Enhanced deep residual networks for single image super-resolution," in *Proc. IEEE Conf. Comput. Vis. Pattern Recognit.*, Jul.2017, pp. 1132-1140.
- [28] R. Timofte, E. Agustsson, "Ntire 2017 challenge on single image super-resolution: Methods and results," in *Proc. IEEE Conf. Comput. Vis. Pattern Recognit. Workshops*, Jul. 2017, vol. 1, pp. 1110-1121.
- [29] Y. Zhao, R. Wang, Y. Chen, W. Jia, X. Liu, W. Gao, "Lighter but efficient bit-depth expansion network," *IEEE Trans. Circuits and Syst. Video Technol.*, vol. 31, no. 5, pp. 2063-2069, 2021.
- [30] H. Zhu, X. Liu, X. Mao, T. Wong, "Real-time deep video deinterlacing," *arXiv preprint*, arXiv:1708.00187, 2017.
- [31] C. Ledig, L. Theis, F. Huszr, "Photo-realistic single image super-resolution using a generative adversarial network," *arXiv preprint*, arXiv:1609.04802, 2016.
- [32] Youku-VSRE dataset, 2019. [Online]. Available: <https://tianchi.aliyun.com/dataset/dataDetail?dataId=39568>
- [33] Methodologies for the subjective assessment of the quality of television images, Rec. ITU-R BT.500, 2019. [Online]. Available: <https://www.itu.int/rec/R-REC-BT.500/en>
- [34] O. Akyüz, "Deep joint deinterlacing and denoising for single shot dual-ISO HDR reconstruction," *IEEE Trans. Image Process.*, vol. 29, pp. 7511-7524, 2020.
- [35] Y. Liu, X. Zhang, S. Wang, S. Ma, W. Gao, "Spatial-temporal correlation learning for real-time video deinterlacing," in *Proc. IEEE Int. Conf. Multimedia and Expo*, 2021, pp. 1-6.
- [36] M. Bernasconi, A. Djelouah, S. Hattori, C. Schroers, "Deep Deinterlacing," *SMPTA Annual Technical Conference and Exhibition*, 2020, pp. 1-12.
- [37] Q. Huang, D. Zhao, S. Ma, W. Gao, H. Sun, "Deinterlacing using hierarchical motion analysis," *IEEE Trans. Circuits and Syst. Video Technol.*, vol. 20, no. 5, pp. 673-686, 2010.
- [38] H. Choi, C. Lee, "Motion adaptive deinterlacing with modular neural networks," *IEEE Trans. Circuits and Syst. Video Technol.*, vol. 21, no. 6, pp. 844-849, 2011.
- [39] T. Xue, B. Chen, J. Wu, D. Wei, W. T. Freeman, "Video enhancement with task-oriented flow," *Int. J. Comput. Vision*, vol. 127, no. 8, pp. 1106-1125, 2019.
- [40] S. Nah, S. Baik, S. Hong, et al, "NTIRE 2019 Challenge on Video Deblurring and Super-Resolution: Dataset and Study," in *Proc. IEEE Conf. Comput. Vis. Pattern Recognit. Workshops*, 2019, pp.1-10.
- [41] S. Su, O. Yan, Y. Zhu, et al, "Blindly assess image quality in the wild guided by a self-adaptive hyper network," in *Proc. IEEE Conf. Comput. Vis. Pattern Recognit.*, 2020.
- [42] V. Hosu, H. Lin, T. Sziranyi, D. Saupe, "KonIQ-10k: An ecologically valid database for deep learning of blind image quality assessment," *IEEE Trans. Image Process.*, vol.29, pp.4041-4056, 2020.